Variability Common to First Leaf Dates and Snowpack in the Western Conterminous United States

Gregory J. McCabe*

U.S. Geological Survey, Denver, Colorado

Julio L. Betancourt

U.S. Geological Survey, Reston, Virginia

Gregory T. Pederson

U.S. Geological Survey, Bozeman, Montana

Mark D. Schwartz

University of Wisconsin–Milwaukee, Milwaukee, Wisconsin

Received 9 July 2013; accepted 15 September 2013

ABSTRACT: Singular value decomposition is used to identify the common variability in first leaf dates (FLDs) and 1 April snow water equivalent (SWE) for the western United States during the period 1900–2012. Results indicate two modes of joint variability that explain 57% of the variability in FLD and 69% of the variability in SWE. The first mode of joint variability is related to widespread late winter–spring warming or cooling across the entire west. The second mode can be described as a north–south dipole in temperature for FLD, as well as in cool season temperature and precipitation for SWE, that is closely

* Corresponding author address: Gregory J. McCabe, U.S. Geological Survey, MS 412, Denver, CO 80225.

E-mail address: gmccabe@usgs.gov

DOI: 10.1175/2013EI000549.1

correlated to the El Niño–Southern Oscillation. Additionally, both modes of variability indicate a relation with the Pacific–North American atmospheric pattern. These results indicate that there is a substantial amount of common variance in FLD and SWE that is related to large-scale modes of climate variability.

KEYWORDS: Timing of spring; Snow water equivalent; Western United States

1. Introduction

Across the western United States, accumulated snowpack [snow water equivalent (SWE)] and the phenological timing of spring onset (as measured by plant leaf-out dates) are both sensitive to variations in cool season climate (Cayan 1996; Cayan et al. 2001; Ault et al. 2011). Snowpack has been shown to integrate changes in temperature and precipitation throughout the cool season in a regionally and physiographically complex manner (e.g., Cayan 1996; McCabe and Wolock 1999; Mote et al. 2005; McCabe et al. 2007; McCabe and Wolock 2009; Pederson et al. 2011; Kapnick and Hall 2012; Pederson et al. 2013), whereas the timing of spring onset as determined by first leaf dates (FLDs) appears most sensitive to variations in temperature in the months preceding the start of the growing season (e.g., Schwartz and Reiter 2000; Cayan et al. 2001; Schwartz et al. 2006; McCabe et al. 2012; Ault et al. 2011). Developing a better understanding of the controls on the variability common to both FLD and SWE may lead to enhanced forecasting and modeling capabilities. Moreover, because leaf out and flowering in many mid- to high-latitude species are limited by snow cover (Dunne et al. 2003), the timing of snowmelt and of the accumulated warmth needed to initiate plant growth (FLD) could be integrated to improve continental-scale indices of phenology. Snowpack is an important component of water resources in the western United States, and much work has been done to establish an understanding of the status and trends, as well as climatic controls, on the spatial and temporal variability in SWE and snow cover (McCabe and Legates 1995; McCabe and Wolock 1999; Stewart et al. 2005; Mote 2003; Mote et al. 2005; McCabe and Clark 2005; Knowles et al. 2006; McCabe et al. 2007; Pederson et al. 2011; Kapnick and Hall 2012; Pederson et al. 2013). For snowmelt-dominated basins in the western United States, snowmelt runoff during the spring and early summer can account for 50%–80% of total annual runoff (Serreze et al. 1999; Stewart et al. 2005). In addition to affecting the magnitude of runoff, the melting of snow also affects the timing of runoff and is influenced by synoptic-scale changes in atmospheric circulation (Stewart et al. 2005; McCabe and Clark 2005; Pederson et al. 2011).

Analyses of teleconnections between the ocean/atmosphere and SWE in the western United States indicate that sea surface temperatures and large-scale atmospheric circulation have a strong influence on the regional variability of SWE in the western United States. Clark et al. (Clark et al. 2001) found that El Niño–Southern Oscillation (ENSO) effects on seasonal snowpack evolution were significant for parts of the Columbia and Colorado River basins and provide useful information for predicting annual runoff. Using principal components analysis, McCabe and Dettinger (McCabe and Dettinger 2002) identified two dominant modes of SWE variability in the western United States that explained 61% of the

total variability in SWE. The first mode was found to be closely associated with the Pacific decadal oscillation (PDO), whereas the second mode was related to both PDO and ENSO.

Cayan (Cayan 1996) showed that anomalously low 1 April SWE in the western United States was related to a positive Pacific–North American (PNA) circulation pattern (Barnston and Livezey 1987; Leathers et al. 1991; Leathers and Palecki 1992): that is, an atmospheric pattern with an anomalously strong Aleutian low and ridging over the western United States. In a recent study, Abatzoglou (Abatzoglou 2011) reported that a positive trend in the late winter PNA over the last half century contributed to regional increases in the elevation of the freezing level, decreases in the percent of precipitation falling as snow, and increases in snowmelt across the western United States. In another study, Pederson et al. (Pederson et al. 2013) also suggest that about 20%–50% of the decline in western U.S. snowpack, especially since the 1980s, may be due to natural variability associated with the PNA pattern, the northern annular mode (NAM), and ENSO. Both of these studies suggest that the PNA has reinforced warming over the western United States during recent decades.

Another integrator of climate is the timing of phenological events (seasonal changes in plant and animal activity) (Running and Hunt 1993; Myneni et al. 1997; Schwartz 1997; Schwartz 1998; Menzel and Fabian 1999; Sparks and Crick 1999; Schwartz and Reiter 2000; Cayan et al. 2001; Parmesan and Yohe 2003; Menzel et al. 2006; Schwartz et al. 2006). For example, the spring indices ''suite of metrics'' (Schwartz and Reiter 2000) use weather-based phenological models of lilac (*Syringa chinensis* ''Red Rothomagensis'') and honeysuckle (*Lonicera tatarica* ''Arnold Red'' and *L. korolkowii* ''Zabeli''), validated with continental-scale phenological observations, as proxies for the occurrence of first leaf, first bloom, and other temperature-sensitive phenological responses to climate. Further, these spring indices (SI) provide an effective approach for integrating climate data into metrics that are broadly representative of many deciduous plant species in temperate regions and thus provide a long-term (1900–2012) and spatially widespread dataset of relevant phenological indicators (Schwartz et al. 2013).

Analyses of time series of SI first leaf and first bloom dates for sites across North America have identified regional differences in the variability of these phenological indicators and have indicated long-term trends toward an earlier onset of spring associated with warming temperatures, especially for the northwestern United States. (Schwartz and Reiter 2000). As might be expected, these trends are evident in monthly averages of springtime temperatures and actual phenological observations made for lilac and honeysuckle since 1956 (Cayan et al. 2001).

Spatiotemporal variability in the timing of spring across North America and the continental United States arises from complex climatic variations synthesized by indices of large-scale sea surface temperature (SST) or atmospheric pressure patterns similar to those found to be important for the evolution of western U.S. snowpack. Because ocean–atmosphere indices can summarize complex and sequenced weather and climatic conditions into a single value, phenologists have started to employ these indices in explaining phenophase variations for both plants and animals (Cayan et al. 2001; Stenseth et al. 2003; Hallet et al. 2004; Gordo 2007; McCabe et al. 2012). For example, McCabe et al. (McCabe et al. 2011) examined relations between FLDs and ENSO and PDO. They found that, although

spring (mean March–April) ENSO and PDO signals are apparent in first leaf dates, the signals are not statistically significant [at a 95% confidence level ($p < 0.05$)] for most sites. However, an analysis of the spatial distributions of first leaf dates for separate and combined ENSO/PDO conditions features a northwest–southeast dipole that is significantly (at $p < 0.05$) different from the distributions for neutral conditions. They also found that the nature of the teleconnections between Pacific Ocean SSTs and FLDs is evident in composites of sea level pressure (SLP) anomalies for spring months. During positive ENSO/PDO, there is an anomalous flow of warm air from the southwestern United States into the northwestern United States and an anomalous northeasterly flow of cold air from polar regions into the eastern and southeastern United States. These flow patterns are reversed during negative ENSO/PDO. Although the magnitudes of first leaf date departures are not necessarily significantly related to ENSO and PDO, the spatial patterns of departures for ENSO and PDO are statistically significant ($p < 0.05$).

In a related study, Ault et al. (Ault et al. 2011) used FLDs to examine variability in the timing of spring onset in the western United States. They found that two independent atmospheric circulation patterns (i.e., the PNA pattern and the NAM) explain roughly half of the total variance in the timing of spring onset during 1920–2005. The influence of PNA on FLDs is strongest in March, and the influence of NAM is strongest in April. Ault et al. (Ault et al. 2011) suggest that these atmospheric circulation patterns modulate the timing of the onset of spring by influencing the number and intensity of warm days. They showed abrupt advances in FLD after the 1980s, coincident with abrupt increases in both the PNA and the NAM. As with the Abatzoglou (Abatzoglou 2011) study on freezing levels, Ault et al. (Ault et al. 2011) detected significant trends in FLD even after PNA influence was removed.

Previous research thus has indicated that both FLD and SWE are sensitive to climate variability and change, and both are sensitive to variability in similar large-scale modes of climate variability. Because both FLD and SWE have demonstrated common climate sensitivities and forcings, the objective of this study is to identify common variability in FLD and SWE pertaining to large-scale modes of climate variability. Improved understanding of the natural drivers underlying variability in FLD and SWE may lead to improved forecasting and modeling of these important climate integrators.

2. Data and methods

2.1. First leaf dates

A dataset of modeled FLDs and first bloom dates (FBDs) was developed by Schwartz and Reiter (Schwartz and Reiter 2000) and expanded by Schwartz et al. (Schwartz et al. 2006). These first leaf dates (and bloom dates) were computed using a model (SI model) that uses daily minimum and maximum temperatures, and it is calibrated and validated using observations of first leaf and first bloom dates of lilac and honeysuckle. More recently, an extended dataset of conterminous U.S. FLDs and FBDs for the period 1900–2012 was developed by Schwartz et al. (Schwartz et al. 2013). This extended spring index (SI-x) dataset includes FLDs and FBDs for 716 stations from the National Weather Service Cooperative

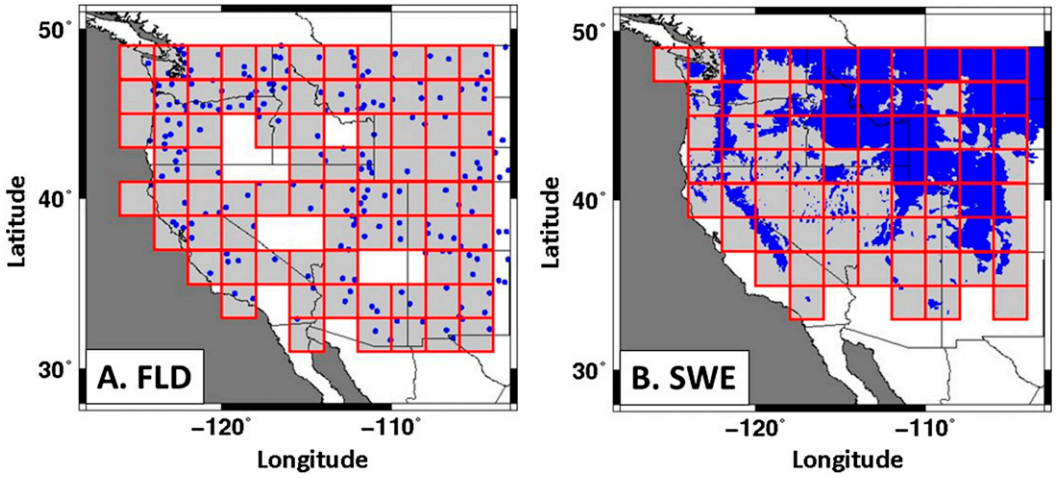

Figure 1. Sites (blue) and 2° by 2° grid cells (red) for (a) FLD and (b) 1 Apr SWE.

Observer Program across the conterminous United States (Figure 1a) and includes the subtropics while retaining the utility and accuracy of the original SI (Schwartz and Reiter 2000; Schwartz et al. 2006). The FLDs used in this study are a model-derived indicator of the onset of spring that integrates a variety of climatological variables (Schwartz and Reiter 2000). Comparison of the SI-x and the original SI for FLDs and FBDs (not shown) indicates substantial similarity between the four datasets (Schwartz et al. 2013). The analysis presented in this study uses the SI-x index for FLDs.

The number of sites (out of 716) with SI-x FLDs in any given year ranges from 246 to 690 during the 1900–2012 period, with a median value of 606 sites. To provide century-long time series of FLDs for all 716 sites, missing data for individual sites were filled using a regression approach. For each year, a regression was developed between FLDs (the dependent variable) for sites with data and the latitude, longitude, and elevation for these sites (the independent variables). The regression then was used to estimate FLDs for sites with missing data. The distribution of coefficients of determination for the regressions for each year indicated reliable regression models. The coefficients of determination had a median value of 0.87, a 25th percentile of 0.85, and a 75th percentile of 0.88. Using the yearly regression models to fill in the missing FLDs resulted in 716 sites in the conterminous United States with complete FLD time series for 1900–2012.

2.2. Snow water equivalent

Because most SWE measurements began in the mid-twentieth century, we use a snow model to estimate SWE for locations in the western United States during the 1900–2012 period. To compute SWE, monthly temperature and precipitation data for the period January 1895–December 2012 were obtained from the Parameter-Elevation Regression on Independent Slopes Model (PRISM) dataset (http://www.ocs.orst.edu/prism/). These data are provided on a 4-km by 4-km grid. Temperature

and precipitation data for grid cells in the western United States (west of 102°W: 209 584 PRISM grid cells) were used as input to a monthly time step snow accumulation and melt model (snow model), which was used to estimate monthly SWE at each grid cell. Model-estimated SWE for the years 1900–2012 were used for analysis. SWE estimates for 1895–99 were discarded to avoid effects of initial model conditions on SWE estimates.

Hydrologic models have been used in a number of studies to simulate snow cover, depth, and water equivalent (Hamlet et al. 2005; McCabe and Wolock 1999; Mote et al. 2005; McCabe and Wolock 2008). The snow model used in this study is based on concepts previously used in monthly water balance models (McCabe and Ayers 1989; Tarboton et al. 1991; Tasker et al. 1991; McCabe and Wolock 1999; Wolock and McCabe 1999; McCabe and Wolock 2008). Inputs to the model are monthly temperature T and precipitation P; the occurrence of snow is computed as

$$S = \begin{cases} P & \text{for} \quad T_a \leq T_{\text{snow}} \\ P\left(\dfrac{T_{\text{rain}} - T_a}{T_{\text{rain}} - T_{\text{snow}}}\right) & \text{for} \quad T_{\text{snow}} < T_a < T_{\text{rain}}, \\ 0 & \text{for} \quad T_a \geq T_{\text{rain}} \end{cases} \tag{1}$$

where S is monthly snow water equivalent in millimeters, P is monthly precipitation in millimeters, T_a is monthly air temperature in degrees Celsius, T_{rain} is a threshold above which all monthly precipitation is rain, and T_{snow} is a threshold below which all monthly precipitation is snow. When the monthly air temperature is between T_{rain} and T_{snow}, the proportion of precipitation that is snow or rain changes linearly. Snow accumulation and melt are accounted for in the snow model; snow that occurs during the month is added to the snowpack and is subject to melt if the air temperature is warm enough for snowmelt. Thus, for some cases, snow, rain, and snowmelt can occur in the same month.

Snowmelt is computed using a degree-day method of the following form:

$$M = \alpha(T_{\text{air}} - T_{\text{snow}})d, \tag{2}$$

where M is the amount of snow storage that can be melted in a month, α is a melt rate coefficient, and d is the number of days in a month. This type of snowmelt model has been used in previous research (Rango and Martinec 1995).

Using calibrated parameters ($T_{\text{rain}} = 7.0$°C, $T_{\text{snow}} = -4.0$°C, and $\alpha = 0.47$; McCabe and Wolock 2011), the snow model was used to estimate 1 April SWE (i.e., March SWE) for the years 1900–2012 for each of the PRISM grid cells in the western United States (west of 102°W). The 1 April SWE was chosen for this analysis because for most sites with snow in the western U.S. SWE reaches its peak at about 1 April (Cayan 1996; Serreze et al. 1999; Bohr and Aguado 2001; Clark et al. 2001), and this date approximates the net balance between annual snowfall and cool season melt (Bohr and Aguado 2001). Grid cells with large numbers of years with zero SWE cause numerical problems for some statistical analyses. Therefore, only grid cells with 1 April SWE values (referred to here as 1 April SWE) greater than zero for at least 50% of the years during 1900–2012 were kept

for analysis. This filtering of grid cells provided 75 465 grid cells for analysis (Figure 1b).

2.3. Gridding of data

Because of the large number of sites with SWE data, relative to the FLD data, and for computational efficiency during analyses, the FLD and SWE data were interpolated to a 2° × 2° grid (Figure 1). The process involved computing simple averages of all data points within each 2° × 2° grid cell. A grid cell had to have at least one site located within it to be retained. Additionally, the grid cells selected for analysis had to include data for each year during 1900–2012. Before computing grid cell average values the individual time series of FLD and SWE were converted to z scores. By converting the original data time series to time series of z scores, the effects of differences in FLD and SWE due to differences in climatic means, elevation, and aspect were removed. Thus, interannual variability in FLD and SWE could be the focus of the analyses. The gridding to 2° × 2° cells resulted in 77 of the 2° × 2° grid cells with complete data for FLD and 72 of the 2° × 2° grid cells with complete data for SWE data (Figure 1). After gridding, there are 63 grid cells that are common to both the FLD and SWE datasets. Although the gridding of data removes some of the variability across space, the spatial variability in FLD and SWE that responds to hemispheric-scale interannual climate variability is preserved for analysis (McCabe et al. 2012).

2.4. Singular value decomposition

A singular value decomposition (SVD) of the joint FLD and SWE gridded datasets was performed to identify the common modes of variance between the FLD and SWE data (Enfield and Alfaro 1999; McCabe and Palecki 2006). Singular value decomposition isolates dominant modes of cross covariance between datasets (Enfield and Alfaro 1999) and has been used in a number of climatic studies (Enfield and Alfaro 1999; McCabe and Palecki 2006; McCabe and Wolock 2010). A detailed discussion of SVD and example application can be found in Bretherton et al. (Bretherton et al. 1992) and Wallace et al. (Wallace et al. 1992). SVD analysis involves an eigenvector decomposition of the cross-covariance matrix between two input fields or variables. Similar to empirical orthogonal function (EOF) analysis, SVD analysis decomposes the variability of the input variables into modes of decreasing explained cross covariance between variables, rather than modes of variability of a single variable as is done with EOF analysis. SVD produces two series of expansion coefficients (i.e., time series) that describe the weighting of each mode on the two input variables. Additionally, correlations between the SVD expansion coefficients and the time series of the original variables (i.e., heterogeneous correlations) provide a way to examine the spatial relations between the SVD modes and the input variables. The expansion coefficients (i.e., time series) of the dominant SVD modes and the patterns of heterogeneous correlations between the SVD modes and FLD and SWE time series for the 2° × 2° grid cells were examined to identify the variability in FLD and SWE represented by the SVD modes.

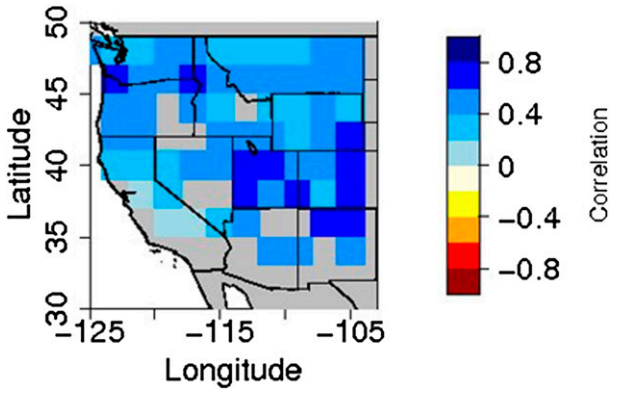

Figure 2. Correlations between first leaf dates and 1 Apr snow water equivalent for 2° by 2° grids during 1900–2012.

3. Results and discussion

A preliminary analysis of the possible covariability between FLD and SWE was performed by correlating FLD and SWE time series for the 2° × 2° grid cells common to both the FLD and SWE datasets (63 grid cells). Positive correlations for all of the common grid cells indicate that, when SWE is higher than average, FLD is later than average (Figure 2). The correlations are statistically significant at $p < 0.05$ for 60 (95%) of the 63 grid cells and are statistically significant at $p < 0.10$ for 62 (98%) of the 63 grid cells. These correlations indicate that there likely is substantial variability common to the FLD and SWE data.

The SVD analysis of the FLD and SWE data resulted in two primary modes of FLD and SWE variability. The first SVD (SVD1) mode explains 42% of the variability in FLD and 51% of the variability in SWE. The second SVD mode (SVD2) explains 15% of the variability in FLD and 18% of the variability in SWE. These two SVD modes were retained because they explain at least 10% of the variability in both FLD and SWE. The total variability explained by the first two SVD modes is 57% for FLD and 69% for SWE. These results indicate that a substantial portion of the variability in FLD and SWE is explained by these two SVDs.

The correlations between the SVD1 expansion coefficients and time series of FLD and SWE time series indicate negative correlations across the western United States (Figures 3a,b). The western-wide negative correlations indicate a similar response of FLD and SWE across the entire western United States to a climatic forcing. Given that both FLD and SWE are sensitive to temperature, it is likely that SVD1 represents the response of FLD and SWE to variability in temperature; higher (lower) than average temperatures result in earlier (later) FLD and decreased (increased) SWE.

Additional analyses were performed to determine the season during which temperature was most strongly related to variability in FLD and SWE. To accomplish this task correlations between SVD1 expansion coefficients for FLD and SWE with mean temperature for the western United States were computed for September–November (SON), October–December (OND), November–January

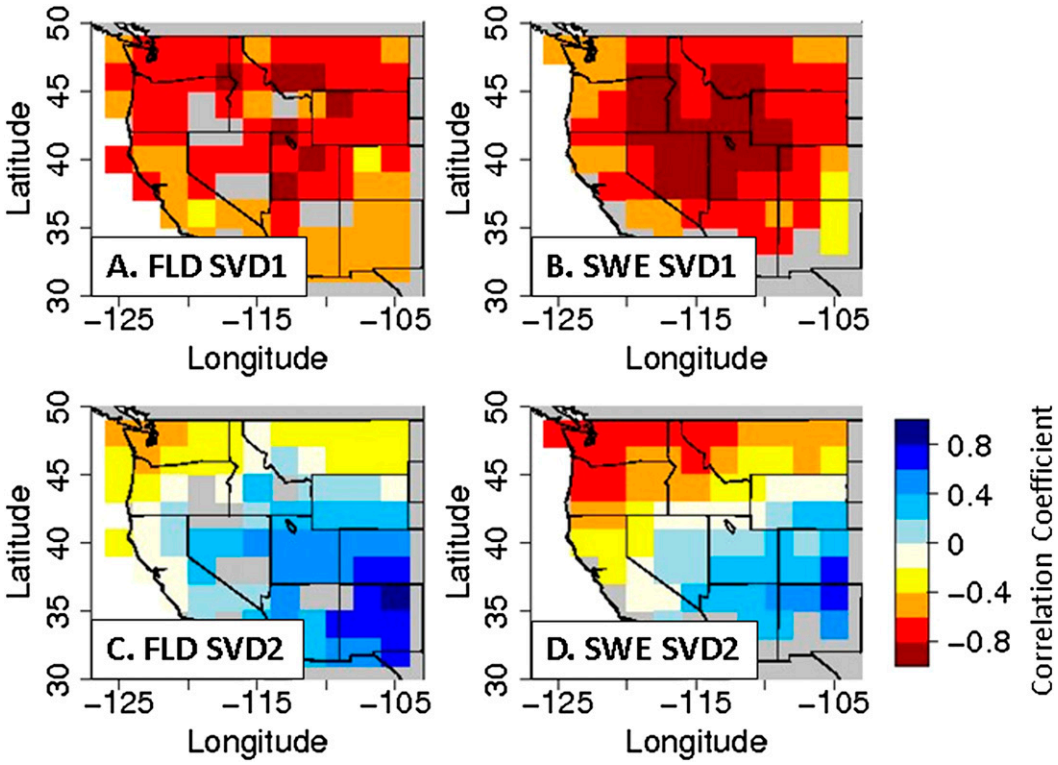

Figure 3. Heterogeneous correlations between SVD1 and SVD2 of FLD and SWE and gridded FLD and SWE time series.

(NDJ), December–February (DJF), January–March (JFM), February–April (FMA), and March–May (MAM) (Figure 4). The correlations between mean western U.S. temperatures and SVD1 (for FLD and SWE) increase from the early fall to mid-winter with a peak correlation for FLD of 0.91 ($p < 0.01$) in JFM and highest correlations for SWE of 0.82 ($p < 0.01$) in DJF and JFM. Figure 5a illustrates the relations between SVD1 expansion coefficients (for FLD and SWE) and JFM temperature. The correlation between FLD SVD1 and SWE SVD1 expansion coefficients is 0.73 ($p < 0.01$), and as noted above the correlations between JFM temperature and the SVD1 expansion coefficients for FLD and SWE are 0.91 and 0.82, respectively.

The relationship between JFM temperature and FLD and SWE that we have shown also may be due to, in part, variability in the PNA pattern. The correlations between JFM PNA and SVD1 for FLD and SWE for the 1900–2012 period are 0.35 ($p < 0.01$) and 0.42 ($p < 0.01$), respectively. Additionally, the correlation between mean JFM temperature for the western United States and mean JFM PNA is 0.44 ($p < 0.01$). These results are consistent with those of Ault et al. (Ault et al. 2011), who reported a relation between variability in FLD and the PNA.

Since both temperature and precipitation are important for plants and snow, an analysis of the correlations between seasonal precipitation and the expansion coefficients for FLD SVD1 and SWE SVD1 were examined. Correlations between

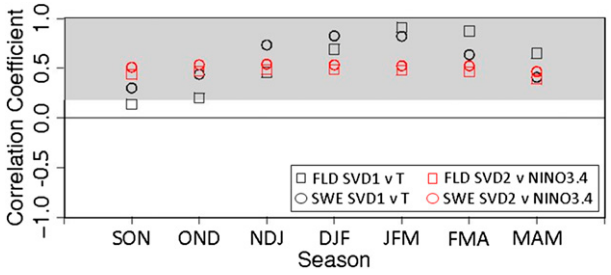

Figure 4. Correlations between seasonal western United States temperature *T* and Niño-3.4 sea surface temperatures and the expansion coefficients SVD1 and SVD2 of FLD and 1 Apr SWE. The seasons are September–November, October–December, November–January, December–February, January–March, February–April, and March–May. Symbols in the gray-shaded region indicate correlations that are statistically significant at $p < 0.05$.

seasonal precipitation and FLD SVD1 and SWE SVD1 are near zero or negative and generally are much less significant than those for temperature (Figure 6). For FLD SVD1, none of the precipitation correlations were statistically significant (at $p < 0.05$). Since the SVD1 expansion coefficients are negatively correlated with both FLD and SWE (Figures 3a,b), negative correlations between SVD1 and precipitation indicate that when precipitation is above average FLD is later and SWE is larger. For SWE SVD1 there were statistically significant (at $p < 0.05$) correlations with precipitation for the NDJ, DJF, and JFM seasons; however,

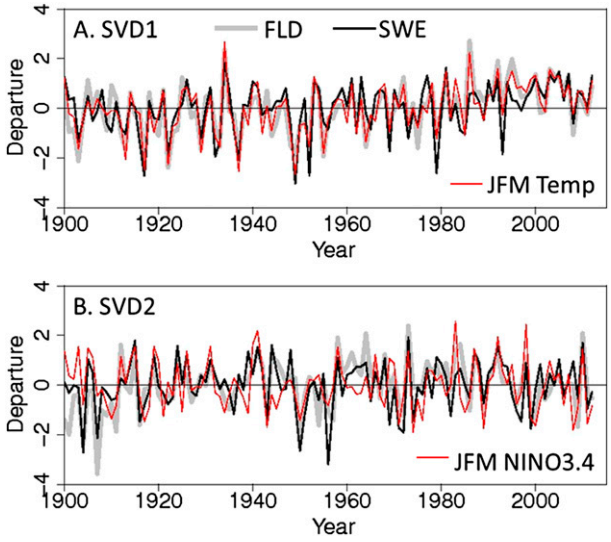

Figure 5. Expansion coefficients for SVD1 and SVD2 of FLD and 1 Apr SWE and time series of JFM mean western United States temperature and JFM Niño-3.4 sea surface temperatures.

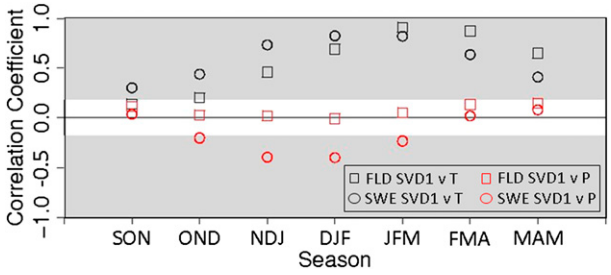

Figure 6. Correlations between seasonal western United States temperature *T* and precipitation *P* and the expansion coefficients of SVD1 of FLD and 1 Apr SWE. The seasons are September–November, October–December, November–January, December–February, January–March, February–April, and March–May. Symbols in the gray-shaded regions indicate correlations that are statistically significant at $p < 0.05$.

correlations of SWE SVD1 with temperature for these same seasons were more statistically significant and all were above 0.7 (Figure 6).

The correlations between the SVD2 expansion coefficients and time series of FLD and SWE for the 2° × 2° grid cells indicate negative correlations for the northwestern United States and positive correlations for the southwestern United States (Figures 3c,d). These patterns of correlations are similar to the pattern of the effects of ENSO on U.S. hydroclimate (Redmond and Koch 1991; McCabe and Dettinger 1999).

To examine the relations between ENSO and SVD2 for FLD and SWE we computed correlations between the SVD2 expansion coefficients and an index of ENSO (i.e., Niño-3.4 SSTs, computed as the average of SSTs for the region 5°S–5°N, 170°–120°W). The SST data were obtained from the Kaplan SST dataset (http://www.esrl.noaa.gov/psd/data/gridded/data.kaplan_sst.html). The correlations between seasonal Niño-3.4 SSTs (i.e., SON, OND, NDJ, JFM, FMA, and MAM seasons) and the expansion coefficients of SVD2 for FLD and SWE are relatively consistent (near a correlation of 0.5, $p < 0.01$) from the early fall through the winter season (Figure 4). Since the seasonal correlations between SVD2 and Niño-3.4 SSTs are similar, we selected JFM Niño-3.4 SSTs for use in the remainder of the study to be consistent with the use of JFM temperatures that are highly correlated with SVD1. Figure 5b illustrates the relations between SVD2 for FLD and SWE and JFM Niño-3.4 SSTs. The correlation between the FLD SVD2 and SWE SVD2 expansion coefficients is 0.73 ($p < 0.01$), and the correlations between JFM Niño-3.4 SSTs and the expansion coefficients for FLD SVD2 and SWE SVD2 are 0.48 and 0.52, respectively.

Given the positive correlations between Niño-3.4 SSTs and the expansion coefficients for SVD2, the patterns of correlations between the SVD2 expansion coefficients and FLD and SVD time series (Figures 3c,d) suggest that, when Niño-3.4 SSTs are positive (i.e., El Niño conditions), FLD is earlier than average and SWE is lower than average in the northwestern United States and FLD is later than average and SWE is higher than average in the southwestern United States. These relations occur because during El Niño conditions precipitation generally is below

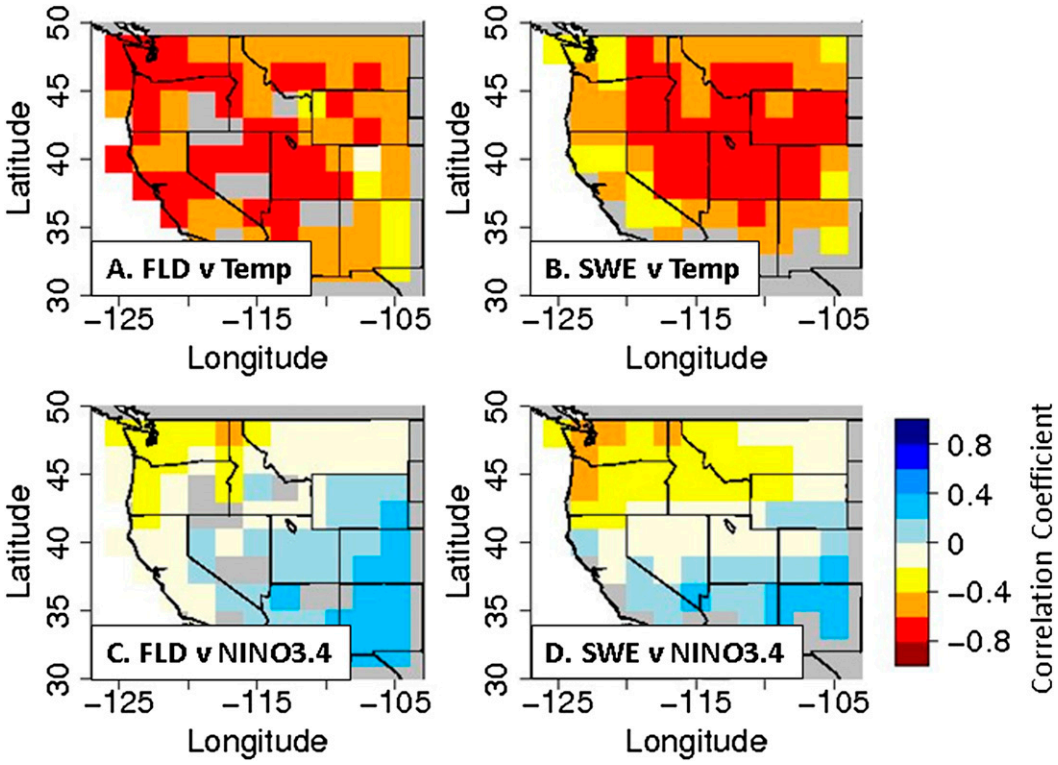

Figure 7. Correlations between mean January–March western United States temperature and (a) FLD and (b) 1 Apr SWE for 2° by 2° grids across the western United States and correlations between mean JFM Niño-3.4 sea surface temperatures and (c) FLD and (d) SWE.

average and temperatures generally are above average in the northwestern United States and precipitation is above average and temperatures are cooler than average across the southwestern United States (Redmond and Koch 1991; McCabe and Dettinger 2002). These climatic conditions are conducive to earlier FLD and decreased SWE in the northwestern United States and later FLD and increased SWE in the southwestern United States. Opposite precipitation and temperature anomaly patterns, as well as associated FLD and SWE conditions, occur during negative Niño-3.4 conditions (i.e., La Niña conditions).

Correlations of JFM temperature and JFM Niño-3.4 time series with the 2° × 2° gridded FLD and SWE time series (Figure 7) indicate patterns that are similar to the patterns of correlations between the expansion coefficients for SVD1 and SVD2 and the FLD and SWE time series (Figure 3). For example, the correlations between the patterns in Figure 3 with the associated patterns in Figure 7 (i.e., Figures 3a and 7a; Figures 3b and 7b; Figures 3c and 7c; and Figures 3d and 7d) are 0.90, 0.82, 0.92, and 0.87, respectively. All of these correlations are statistically significant at $p < 0.01$.

To support the interpretation presented here of the climatic causes of the relations between SVD1 and JFM temperature and SVD2 and Niño-3.4 temperatures,

we examined these relations in the context of atmospheric pressure anomalies. To do this, we computed correlations between JFM 700-hPa heights and the time series of SVD1, SVD2, JFM temperature, and JFM Niño-3.4 SSTs. We selected 700-hPa heights for this analysis because the 700-hPa pressure surface is about 3000 m above mean sea level and provides a good representation of midtropospheric atmospheric circulation, which controls seasonal weather variations (Cayan 1996; McCabe and Dettinger 2002). Monthly 700-hPa data were obtained from the National Oceanic and Atmospheric Administration (NOAA)/Earth System Research Laboratory (ESRL) (http://www.esrl.noaa.gov/psd/data/gridded/data.ncep.reanalysis.pressure.html) for the period 1948–2012. Mean JFM 700-hPa data were computed from the monthly data.

Correlations between the SVD1 time series and JFM 700-hPa heights (Figures 8a,c) indicate negative correlations over the northeastern Pacific Ocean and positive correlations over the western United States. This pattern indicates that, when SVD1 is positive, 700-hPa heights are higher than average (i.e., higher than average atmospheric pressures) over the western United States. The higher than average heights over the western United States are associated with anomalously warm temperatures and a northward displacement of storm tracks and precipitation. Correlations between mean JFM temperatures and 700-hPa heights (Figure 8e) are consistent with this explanation and show a pattern of correlations that is similar to the pattern of correlations between SVD1 and JFM 700-hPa heights (Figures 8a,c).

The correlations between SVD1 time series and JFM 700-hPa heights provide an explanation for the patterns of correlations of SVD1 with FLD and SWE time series (Figures 3a,b). The correlations between SVD1 and FLD and SWE indicate that when SVD1 is positive FLD dates are earlier and SWE is lower than average (Figures 3a,b). These relations are consistent with increased JFM temperature over the western United States when SVD1 is positive (and JFM 700-hPa heights are higher than average).

Correlations between the SVD2 time series for FLD and SWE and 700-hPa heights indicate positive correlations over western Canada and the northwestern United States, with negative correlations that extend from the northeastern Pacific Ocean across the southern United States to the North Atlantic Ocean (Figures 8b, d). This pattern of correlations matches the pattern of correlations of JFM Niño-3.4 with JFM 700-hPa heights (Figure 8f). The similarity of the correlation patterns for the SVD2 time series (Figures 8b,d) and Niño-3.4 (Figure 8e) support the interpretation that SVD2 represents the teleconnections of ENSO with FLD and SWE across the western United States.

In a principal component analysis of FLD (1920–2005) across western North America, Ault et al. (Ault et al. 2011) found statistically significant relations between FLDs and the PNA and NAM, strongest in March and April, respectively, and associated with the local frequency and intensity of warm days (synoptic events). The relation between PNA and FLD is consistent with the results presented here for Niño-3.4, because Niño-3.4 SSTs and PNA are related. When Niño-3.4 SSTs are warmer (cooler) than average, PNA is generally in a positive (negative) phase. The correlations between JFM PNA and FLD SVD2 and SWE SVD2 for the 1900–2012 period are 0.53 and 0.55, respectively, compared with correlations of 0.48 and 0.52 for Niño-3.4 SSTs (these correlations are significant at $p < 0.01$).

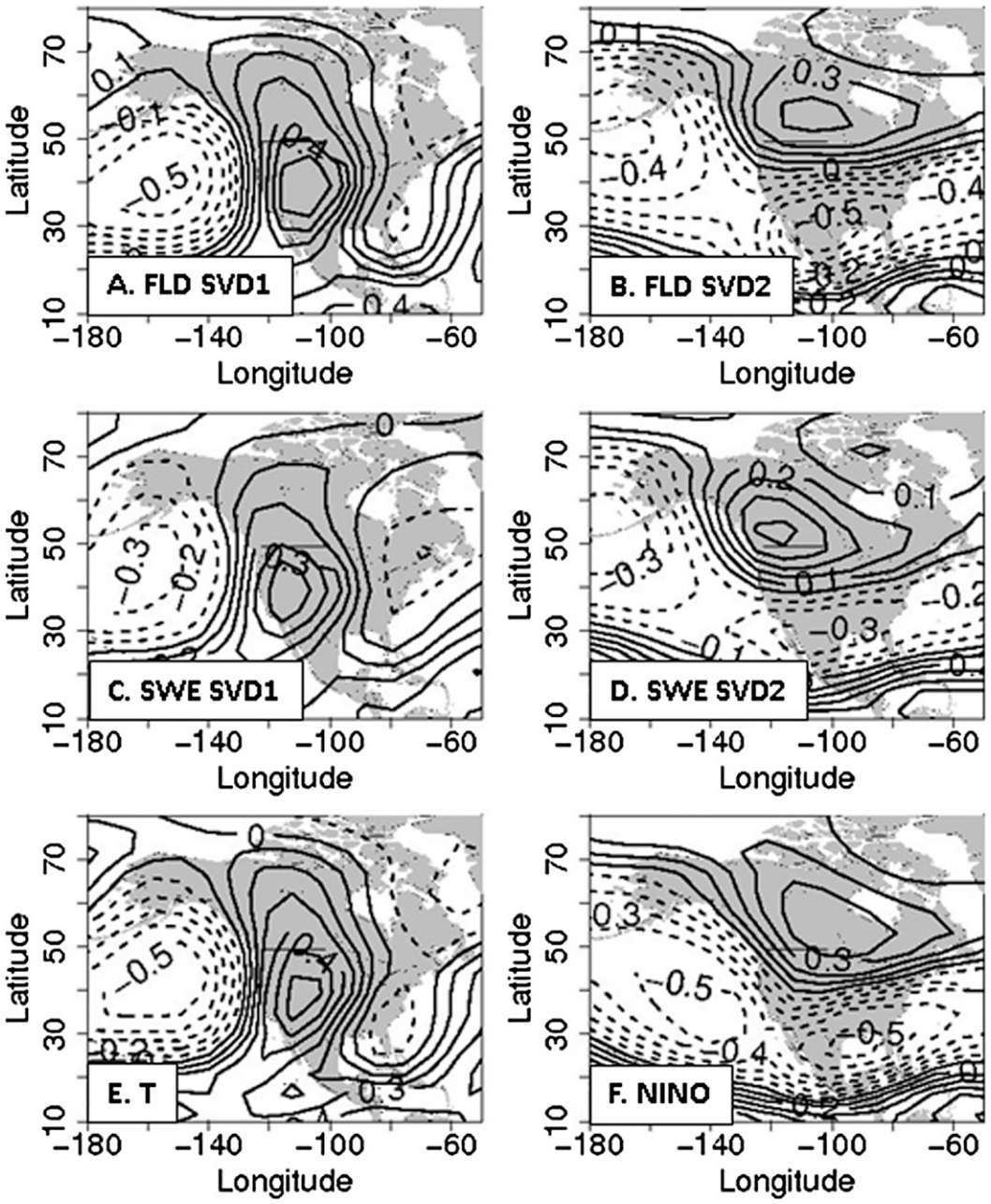

Figure 8. Correlations (indicated by isolines) between mean JFM 700-hPa heights and time series of SVD1 and SVD2 of (a)–(d) FLD and March SWE, (e) mean JFM temperature *T* averaged for the western United States, and (f) mean JFM Niño-3.4 sea surface temperatures. Solid isolines indicate positive correlations and dashed lines indicate negative correlations. The contour interval is 0.1.

In our analyses, we did not see statistically significant correlations between NAM and the FLD and SWE SVDs. The differences in our results compared with those of Ault et al. (Ault et al. 2011) likely exist because they examined FLDs solely, which are based on daily minimum and maximum temperatures and integrate the frequency of synoptic weather events, whereas we examine the variance common to both FLDs and SWE, with the latter based on mean monthly temperature and precipitation. The joint variability of these two climate integrators should be different from the variability of each of the variables alone. For example, we performed principal components analyses of the FLD and SWE data separately and compared the first principal components (PCs) with March NAM (as was done by Ault et al. 2011). The NAM was represented by a time series of the Arctic Oscillation (AO) index. Monthly AO data for 1899–1950 were obtained from the University of Washington's Joint Institute for the Study of the Atmosphere and Ocean (JISAO; http://jisao.washington.edu/data/aots/#data), and monthly AO data for 1951–2012 were obtained from the National Oceanic and Atmospheric Administration/Climate Prediction Center (at http://www.cpc.ncep.noaa.gov/products/precip/CWlink/daily_ao_index/monthly.ao.index.b50.current.ascii). We found that, for the 1950–2005 period (the period used by Ault et al.), the first PC for the FLD data is significantly correlated with March NAM at $p < 0.05$ ($r = 0.354$). In contrast, for the 1900–2012 period, the correlation between the first FLD PC and March NAM was nonsignificant (at $p = 0.05$). Additionally, correlations between the first SWE PC and March NAM were nonsignificant (at $p = 0.05$) for both the 1950–2005 and the 1900–2012 periods.

Because we found JFM temperature to be related to the first mode of joint variance (SVD1) in FLD and SWE, we also examined correlations between JFM temperatures and the first PCs of the FLD and SWE data. Correlations of the first FLD PC with JFM temperatures for both the 1950–2005 and 1900–2012 periods are statistically significant at $p < 0.01$ ($r = 0.89$ for both periods), and the correlations of the first SWE PC with JFM temperatures is 0.71 ($p < 0.01$) for the 1950–2005 period and 0.80 ($p < 0.01$) for the 1900–2012 period. These correlations between the FLD and SWE PCs and JFM temperature support the correlations we present between JFM temperature and time series of SVD1 for FLD and SWE.

4. Conclusions

FLD and 1 April SWE aggregated to 2° resolution horizontal grids across the western United States were analyzed using singular value decomposition to identify the common variance in these two climatically sensitive variables. Results indicate that two modes of variability explain 57% of the variability in FLD and 69% of the variability in SWE. The first mode of variability resulting from the SVD analysis reflects the effects of winter temperature on FLD and SWE, whereas the second mode of variability is related to variability in ENSO. These results indicate that there is a substantial amount of common variance in FLD and SWE and that this variability largely is explained by variability in temperature and ENSO.

SWE and FLD are presently part of the Environmental Protection Agency's Climate Change Indicators in the United States (http://www.epa.gov/climatechange/science/indicators/) and are under consideration for use in the Indicator System of

the National Climate Assessment (http://www.globalchange.gov/what-we-do/assessment/indicators-system). An obvious next step to our research would be to conduct similar joint variability analyses for a wide suite of related indicators for springtime seasonal timing and phenology, including dates of snowmelt; snowmelt-driven runoff; freeze–thaw in soils, streams, and lakes; accumulated growing degree-days; last frost; and start of the flammable (fire) season. Another extension of our research might be to integrate pairs of related indicators. Patterns for date of snowmelt and FLD, for example, both depend on daily data and probably have similar climatic controls (including ENSO variability), and their integration could enable long-lead forecasts of spring leafing and flowering.

Acknowledgments. The SI models were developed using phenological data that now reside and are available through the National Phenology Database at the USA National Phenology Network. We thank J. T. Abatzoglou for reviewing the manuscript and providing comments that improved the overall quality of the document. Any use of trade, firm, or product names is for descriptive purposes only and does not imply endorsement by the U.S. government.

References

Abatzoglou, J. T., 2011: Influence of the PNA on declining mountain snowpack in the western United States. *Int. J. Climatol.,* **31,** 1135–1142.

Ault, T. R., A. K. Macalady, G. T. Pederson, J. L. Betancourt, and M. D. Schwartz, 2011: Northern Hemisphere modes of variability and the timing of spring in western North America. *J. Climate,* **24,** 4003–4014.

Barnston, A. G., and R. E. Livezey, 1987: Classification, seasonality and persistence of low-frequency atmospheric circulation patterns. *Mon. Wea. Rev.,* **115,** 1083–1126.

Bohr, G. S., and E. Aguado, 2001: The use of April 1 SWE measurements as estimates of peak seasonal snowpack and total cold season precipitation. *Water Resour. Res.,* **37,** 51–60.

Bretherton, C. S., S. Smith, and J. M. Wallace, 1992: An intercomparison of methods for finding coupled patterns in climatic data. *J. Climate,* **5,** 541–560.

Cayan, D. R., 1996: Interannual climate variability and snowpack in the western United States. *J. Climate,* **9,** 928–948.

——, S. A. Kammerdiener, M. D. Dettinger, J. M. Caprio, and D. H. Peterson, 2001: Changes in the onset of spring in the western United States. *Bull. Amer. Meteor. Soc.,* **82,** 399–415.

Clark, M. P., M. C. Serreze, and G. J. McCabe, 2001: The historical effect of El Niño and La Niña events on the seasonal evolution of the montane snowpack in the Columbia and Colorado River basins. *Water Resour. Res.,* **37,** 741–757.

Dunne, J. A., J. Harte, and K. J. Taylor, 2003: Subalpine meadow flowering phenology responses to climate change: Integrating experimental and gradient methods. *Ecol. Monogr.,* **73,** 69–86.

Enfield, D. B., and E. T. Alfaro, 1999: The dependence of Caribbean rainfall on the interaction of the tropical Atlantic and Pacific Oceans. *J. Climate,* **12,** 2093–2103.

Gordo, O., 2007: Why are bird migration dates shifting? A review of weather and climate effects on avian migratory phenology. *Climate Res.,* **35,** 37–58.

Hallett, T. B., T. Coulson, J. G. Pilkington, T. H. Clutton-Brock, J. M. Pemberton, and B. Grenfell, 2004: Why large-scale climate indices seem to predict ecological processes better than local weather. *Nature,* **430,** 71–75.

Hamlet, A. F., P. W. Mote, M. P. Clark, and D. P. Lettenmaier, 2005: Effects of temperature and precipitation variability on snowpack trends in the western United States. *J. Climate,* **18,** 4545–4561.

Kapnick, S., and A. Hall, 2012: Causes of recent changes in western North American snowpack. *Climate Dyn.,* **38,** 1885–1899, doi:10.1007/s00382-011-1089-y.

Knowles, N., M. D. Dettinger, and D. R. Cayan, 2006: Trends in snowfall versus rainfall in the western United States. *J. Climate,* **19,** 4545–4559.

Leathers, D. J., and M. A. Palecki, 1992: The Pacific/North American teleconnection pattern and the United States climate. Part II: Temporal characteristics and index specification. *J. Climate,* **5,** 707–716.

——, B. Yarnal, and M. A. Palecki, 1991: The Pacific/North American teleconnection pattern and United States climate. Part I: Regional temperature and precipitation associations. *J. Climate,* **4,** 517–528.

McCabe, G. J., and M. A. Ayers, 1989: Hydrologic effects of climate change in the Delaware River basin. *Water Resour. Bull.,* **25,** 1231–1242.

——, and D. R. Legates, 1995: Relations between 700-millibar height anomalies and April 1 snowpack accumulations in the western United States. *Int. J. Climatol.,* **15,** 517–530.

——, and M. D. Dettinger, 1999: Decadal variations in the strength of ENSO teleconnections with precipitation in the western United States. *Int. J. Climatol.,* **19,** 1399–1410.

——, and D. M. Wolock, 1999: Future snowpack conditions in the western United States derived from general circulation model climate simulations. *J. Amer. Water Resour. Assoc.,* **35,** 1473–1484.

——, and M. D. Dettinger, 2002: Primary modes and predictability of year-to year snowpack variations in the western United States from teleconnections with Pacific Ocean climate. *J. Hydrometeor.,* **3,** 13–25.

——, and M. P. Clark, 2005: Trends and variability in snowmelt runoff in the western United States. *J. Hydrometeor.,* **6,** 476–482.

——, and M. A. Palecki, 2006: Multidecadal climate variability of global lands and oceans. *Int. J. Climatol.,* **26,** 849–865.

——, and D. M. Wolock, 2008: Joint variability of global runoff and global sea surface temperatures. *J. Hydrometeor.,* **9,** 816–824.

——, and ——, 2009: Recent declines in western U.S. snowpack in the context of twentieth-century climate variability. *Earth Interact.,* **13,** doi:10.1175/2009EI283.1.

——, and ——, 2010: Long-term variability in Northern Hemisphere snow cover and associations with warmer winters. *Climatic Change,* **99,** 141–153.

——, and ——, 2011: Century-scale variability in global annual runoff examined using a water balance model. *Int. J. Climatol.,* **31,** 1739–1748, doi:10.1002/joc.2198.

——, M. P. Clark, and L. E. Hay, 2007: Rain-on-snow events in the western United States. *Bull. Amer. Meteor. Soc.,* **88,** 319–328.

——, T. R. Ault, B. I. Cook, J. L. Betancourt, and M. D. Schwartz, 2012: Influences of the El Niño Southern Oscillation and the Pacific decadal oscillation on the timing of North American spring. *Int. J. Climatol.,* **32,** 2301–2310, doi:10.1002/joc.3400.

Menzel, A., and P. Fabian, 1999: Growing season extended in Europe. *Nature,* **397,** 659.

——, and Coauthors, 2006: European phenological response to climate change matches the warming pattern. *Global Change Biol.,* **12,** 1–8.

Mote, P. W., 2003: Trends in snow water equivalent in the Pacific Northwest and their climatic causes. *Geophys. Res. Lett.,* **30,** 1601, doi:10.1029/2003GL017258.

——, A. F. Hamlet, M. P. Clark, and D. P. Lettenmaier, 2005: Declining mountain snowpack in western North America. *Bull. Amer. Meteor. Soc.,* **86,** 39–49.

Myneni, R. B., C. D. Keeling, C. J. Tucker, G. Asrar, and R. R. Nemani, 1997: Increased plant growth in the northern high latitudes from 1981–1991. *Nature,* **386,** 698–702.

Parmesan, C., and G. Yohe, 2003: A globally coherent fingerprint of climate change impacts in natural systems. *Nature,* **421,** 37–42.

Pederson, G. T., and Coauthors, 2011: The unusual nature of recent snowpack declines in the North American cordillera. *Science,* **333,** 332–335.

——, J. L. Betancourt, and G. J. McCabe, 2013: Regional patterns and proximal causes of the recent snowpack decline in the Rocky Mountains, U.S. *Geophys. Res. Lett.,* **40,** 1811–1826, doi:10.1002/grl.50424.

Rango, A., and J. Martinec, 1995: Revisiting the degree-day method for snowmelt computations. *Water Resour. Bull.,* **31,** 657–669.

Redmond, K. T., and R. W. Koch, 1991: Surface climate and streamflow variability in the western United States and their relationship to large scale circulation indices. *Water Resour. Res.,* **27,** 2381–2399.

Running, S. W., and E. R. Hunt, 1993: Generalization of a forest ecosystem process model for other biomes, BIOME–BGC and an application for global scale models. *Scaling Physiological Processes: Leaf to Globe,* C. Field and J. Ehleringer, Eds., Academic Press, 144–157.

Schwartz, M. D., 1997: Spring index models: An approach to connecting satellite and surface phenology. *Phenology of Seasonal Climates,* H. Lieth and M. D. Schwartz, Eds., Backhuys, 23–38.

——, 1998: Green-wave phenology. *Nature,* **394,** 839–840.

——, and B. E. Reiter, 2000: Changes in North American spring. *Int. J. Climatol.,* **20,** 929–932.

——, R. Ahas, and A. Aasa, 2006: Onset of spring starting earlier across the Northern Hemisphere. *Global Change Biol.,* **12,** 343–351.

——, T. R. Ault, and J. L. Betancourt, 2013: Spring onset variations and trends in the continental USA: Past and regional assessment using temperature-based indices. *Int. J. Climatol.*, **33,** 2917–2922, doi:10.1002/joc.3625.

Serreze, M. C., M. P. Clark, R. L. Armstrong, D. A. McGinnis, and R. L. Pulwarty, 1999: Characteristics of the western U.S. snowpack from snowpack telemetry (SNOTEL) data. *Water Resour. Res.,* **35,** 2145–2160.

Sparks, T., and H. Crick, 1999: The times are a-changing? *Bird Conserv. Int.,* **9,** 1–7.

Stenseth, N., G. Ottersen, J. Hurrell, A. Mysterud, M. Lima, K. Chan, N. Yoccoz, and B. Adlandsvik, 2003: Studying climate effects on ecology through the use of climate indices: The North Atlantic Oscillation, El Niño Southern Oscillation and beyond. *Proc. Biol. Sci.,* **270,** 2087–2096.

Stewart, I. T., D. R. Cayan, and M. D. Dettinger, 2005: Changes in snowmelt runoff timing in western North America under a 'business as usual' climate scenario. *Climatic Change,* **62,** 217–232.

Tarboton, D. G., M. J. Al-Adhami, and D. S. Bowles, 1991: A preliminary comparison of snowmelt models for erosion prediction. *Proc. 59th Annual Western Snow Conf.,* Juneau, AK, Western Snow Conference, 79–90.

Tasker, G., M. Ayers, D. Wolock, and G. McCabe, 1991: Sensitivity of drought risks in the Delaware River basin to climate change. *Proc. Technical and Business Exhibition and Symp.,* Huntsville, AL, . Huntsville Association of Technical Societies, 153–158.

Wallace, J. M., S. Smith, and C. S. Bretherton, 1992: Singular value decomposition of wintertime sea surface temperature and 500-mb height anomalies. *J. Climate,* **5,** 561–576.

Wolock, D. M., and G. J. McCabe, 1999: Effects of potential climatic change on annual runoff in the conterminous United States. *J. Amer. Water Resour. Assoc.,* **35,** 1341–1350.